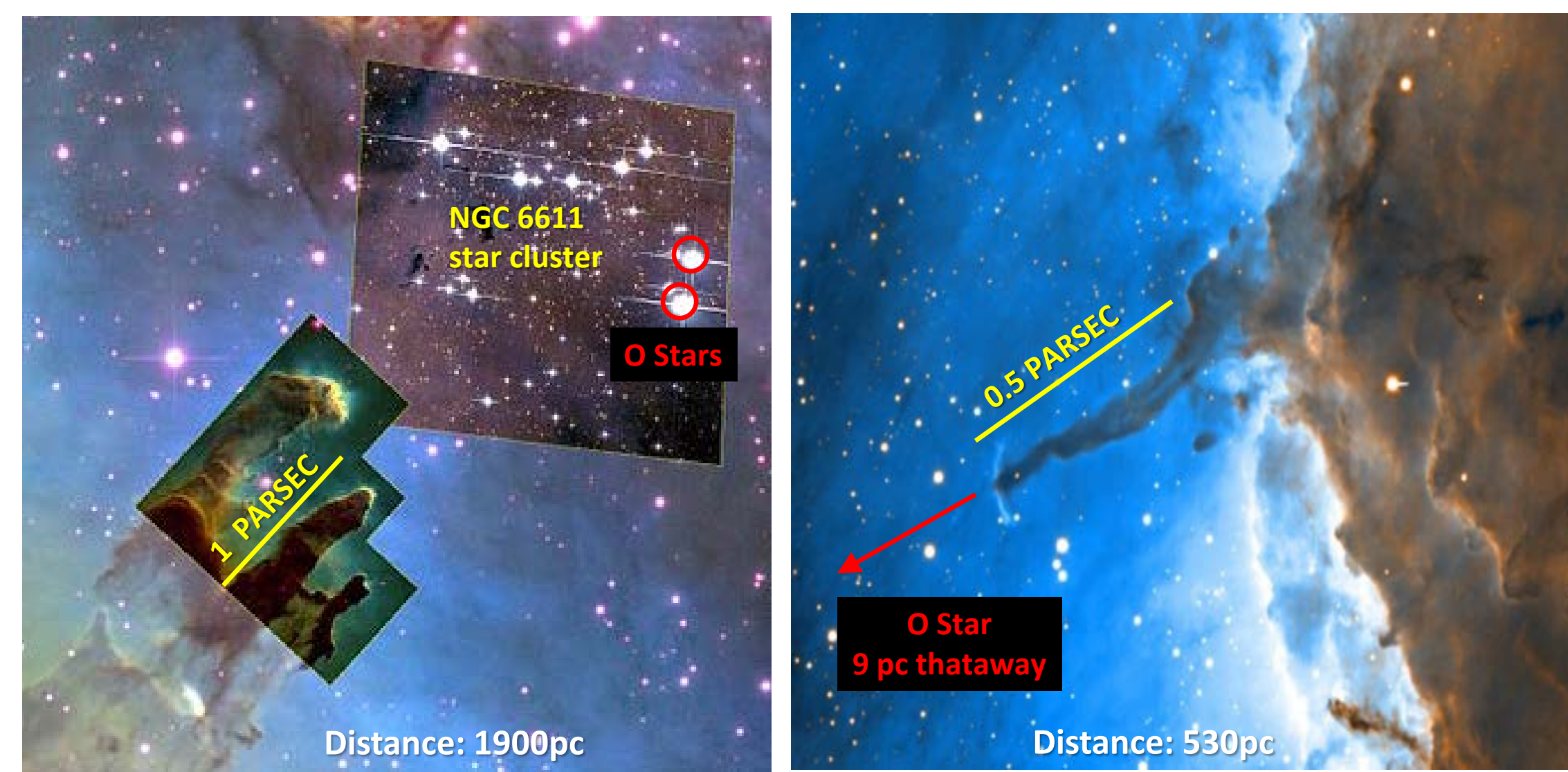


## TWO PILLAR SYSTEMS: EAGLE AND PELICAN

Molecular pillars like those of the Eagle and Pelican nebula are examples of a phenomenon that is commonly seen wherever molecular clouds are situated nears O stars: large “fingers” of gas and dust that point directly back at the highly energetic young stars. Proposed formation mechanisms for such pillars fall into two broad categories: i) instabilities at the boundary between the cloud and the ionized region which grow with time [1,2,3,4,5,6] and ii) pre-existing density enhancements (clumps) which locally retard the ionization front, creating cometary globules [7,8,9].

Though molecular pillars are common, their detailed structure encompasses a wide diversity from relatively smooth to very clumpy or disrupted. We chose to study two systems that have different properties: The Eagle is a multi-pillar, clumpy system close to two O5 stars, while the Pelican is a single, smoother pillar, comparatively far away from an O9 star.

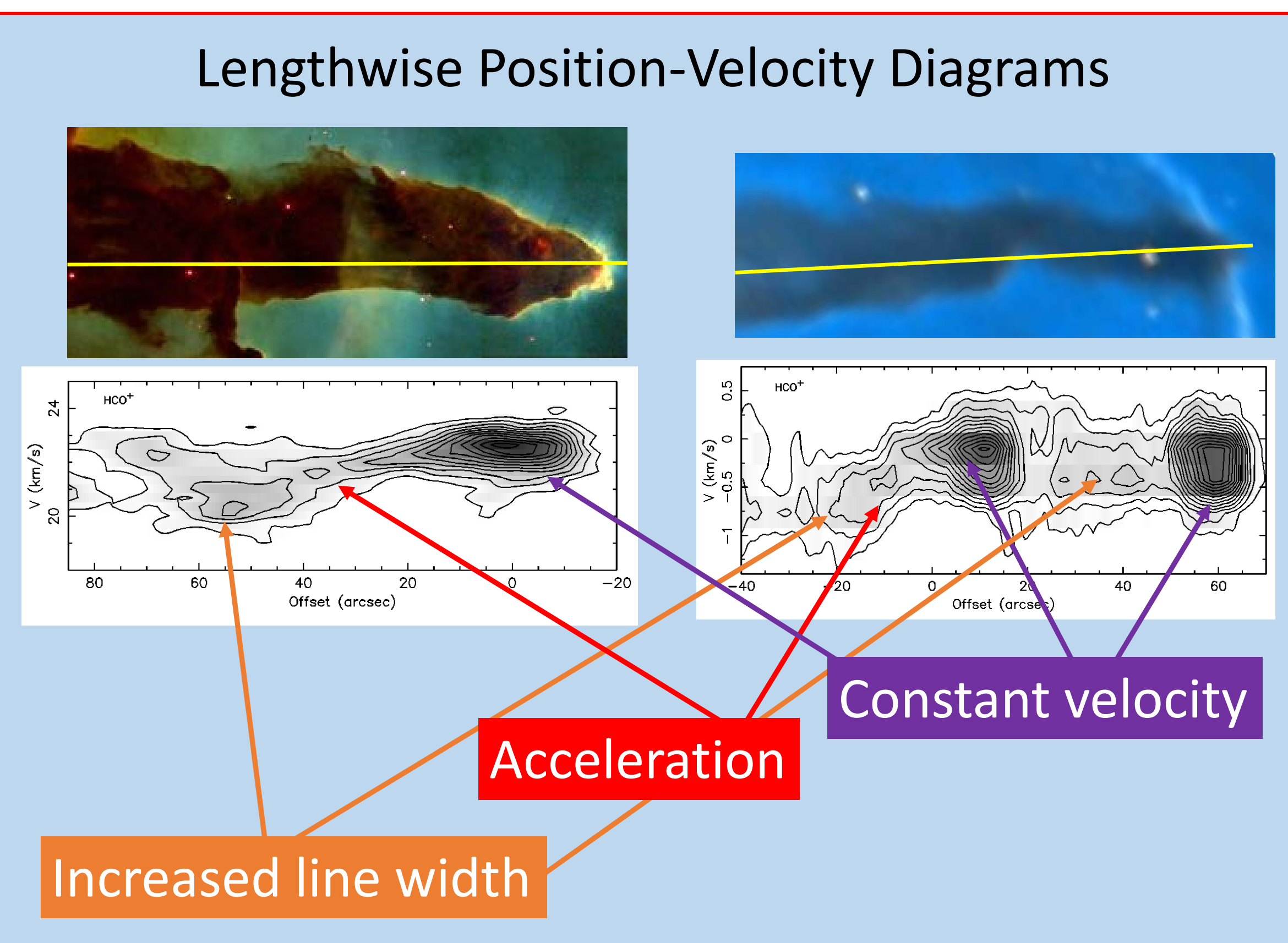


## OBSERVATIONS WITH CARMA

We obtained mm-wavelength observations with The Combined Array for Research in Millimeter-Wave Astronomy to look at the morphology and kinematics of dense gas in these objects. We mapped the 3mm transitions of HCO\*(1-0), HCN(1-0), N<sub>2</sub>H\*(1-0), and CS(2-1) with spectral resolution of 0.08 km/s and spatial resolutions of 9"x6" (Eagle, ~0.07 pc) and 4"x4" (Pelican, ~0.008 pc).



## PILLARS HAVE DISTINCT KINEMATIC SIGNATURES

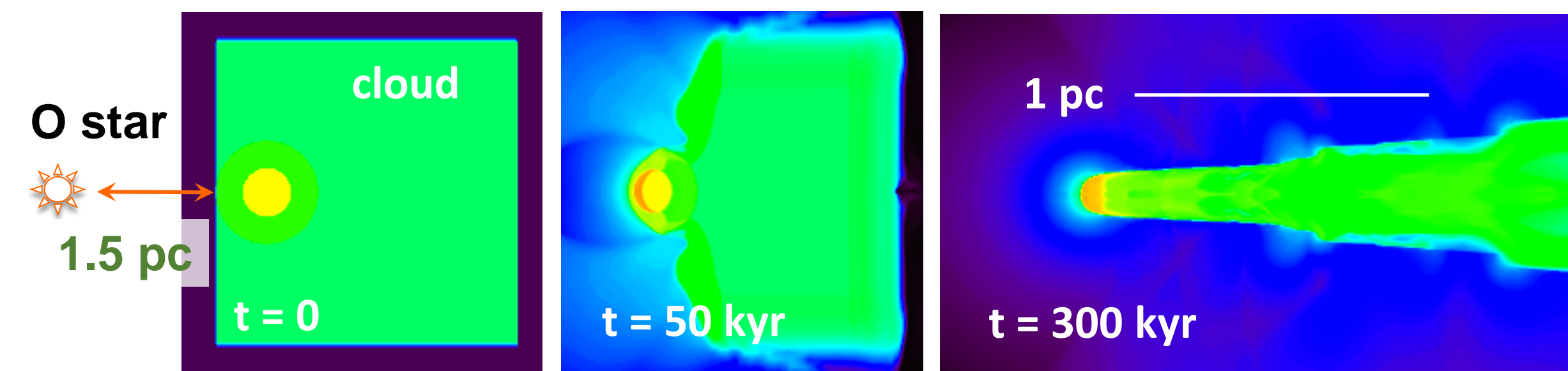


Using CARMA dense gas data, position-velocity cuts along the length of both the Eagle and Pelican pillars show common morphology. Near the denser head, the velocity stays constant, then in the tail there is velocity gradient and line broadening. In the case of the Eagle Pillar II, we know the velocity gradient signifies acceleration not deceleration because it has been shown that Pillar II's head points away from us, its tail towards us [10]. Hence, the same sign on the velocity gradient in the Pelican position-velocity diagram lets us infer its tail must be similarly pointed towards us. The line broadening in the tails suggest gas is pushed past the head into a turbulent wake.

## ASTROPHYSICAL RAD-HYDRO SIMULATIONS

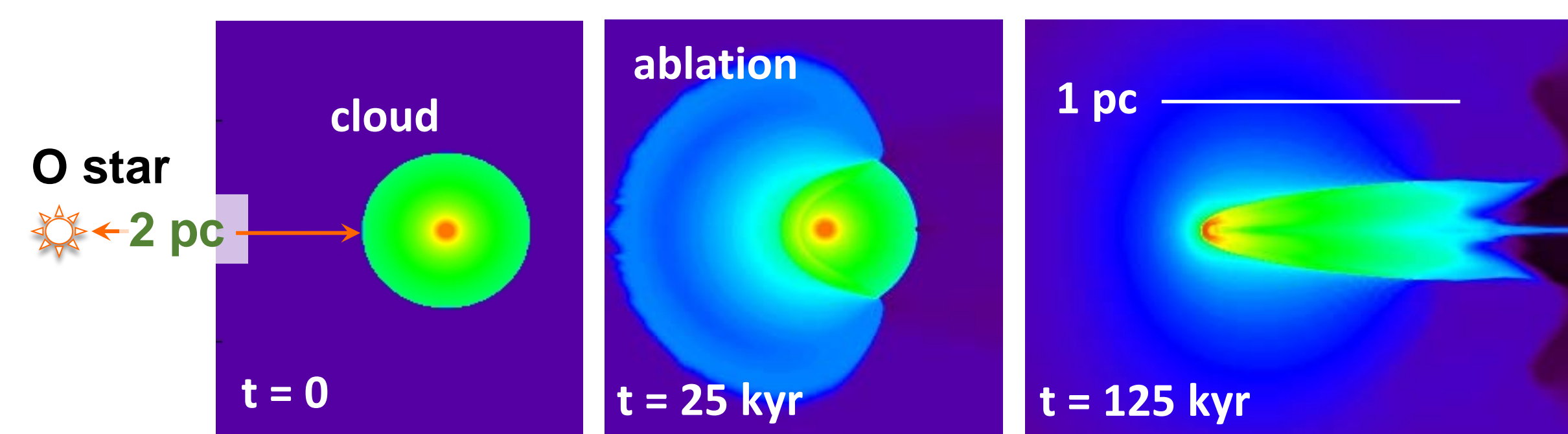
Previously, we developed a 2-D cylindrical geometry radiative hydrodynamics code that includes energy deposition and release due to absorption of UV radiation, hydrogen recombination, radiative molecular cooling, magnetostatic pressure, and geometry and initial conditions based on Eagle observations [1,12]. In the figures below, we show the results of the simulations of two competing models of the origins of pillars: the *shielding* model and the *cometary* model.

### Initial core embedded in uniform cloud (“shielding”)

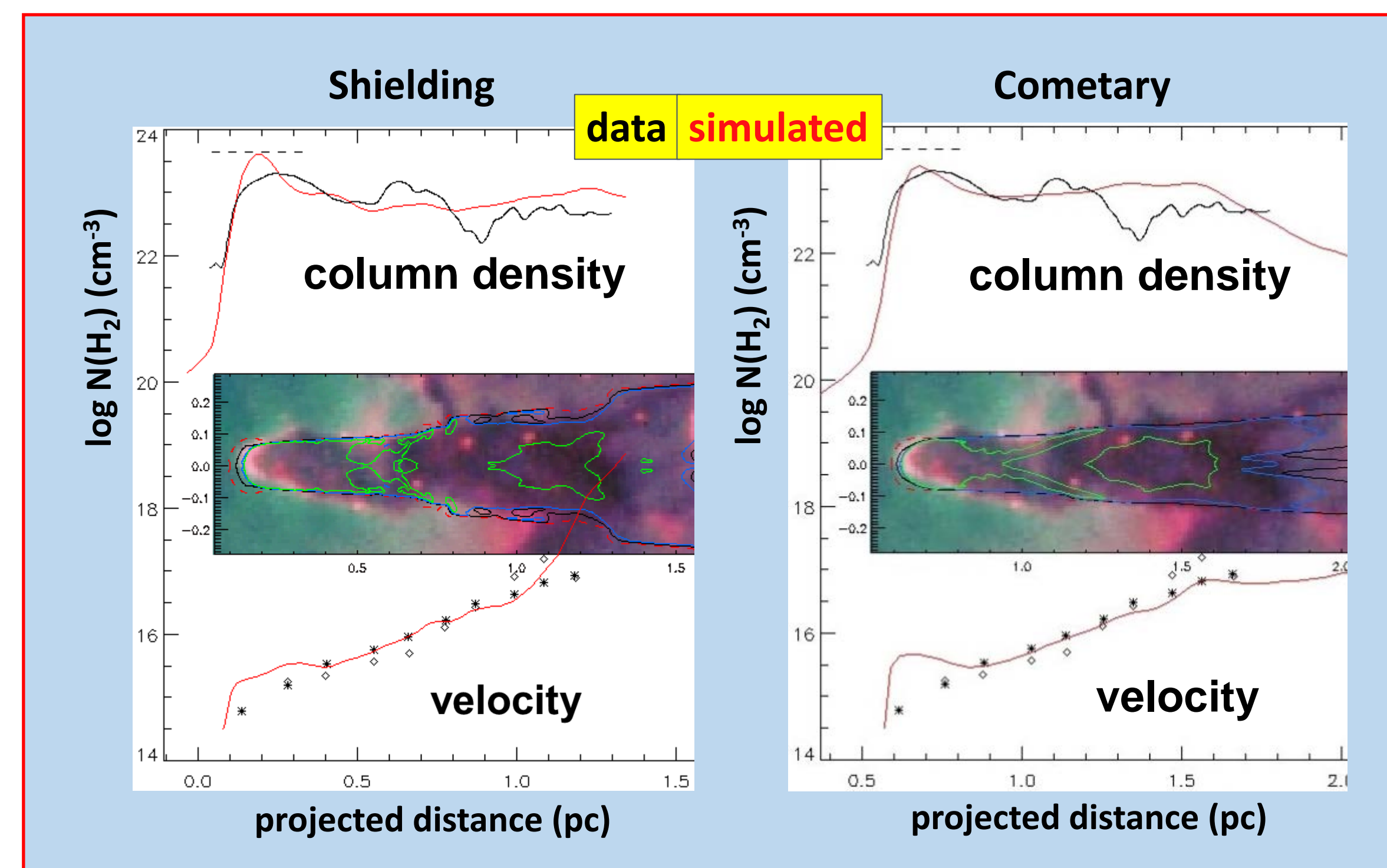


Snapshots of radiative hydrodynamic simulation of the shielding model. A 45 M<sub>⊙</sub> dense molecular core with lower density envelope (total mass 53 M<sub>⊙</sub>) is embedded in a background cloud with volume density n(H) = 1.5E4/cc. An O-type star is situated 1.5 pc away. After 300 kyr, a roughly 2 pc long pillar with dense head has evolved.

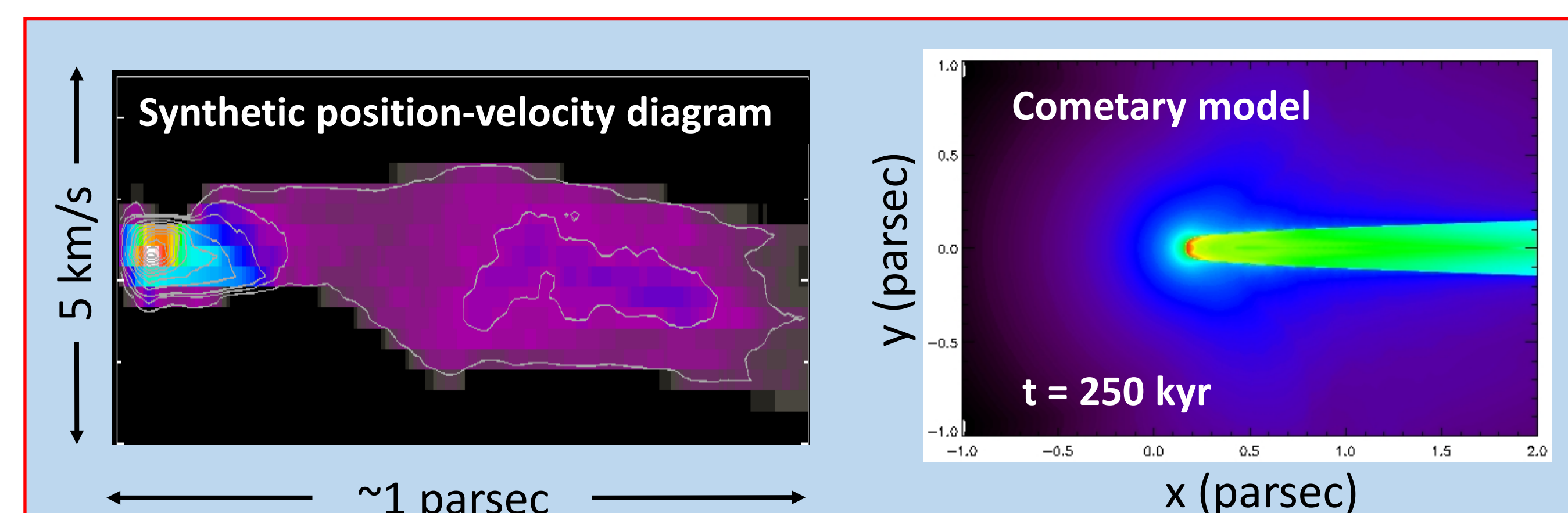
### Spherical cloud with density gradient (“cometary”)



Snapshots of radiative hydrodynamic simulation of the cometary model. A 30 M<sub>⊙</sub> spherical, centrally condensed cloud is irradiated by an O-type star 2 pc away. After 125 kyr, a roughly 1 pc long pillar is seen. After 250 kyr (See below), the pillar has elongated to 2 pc and thinned.



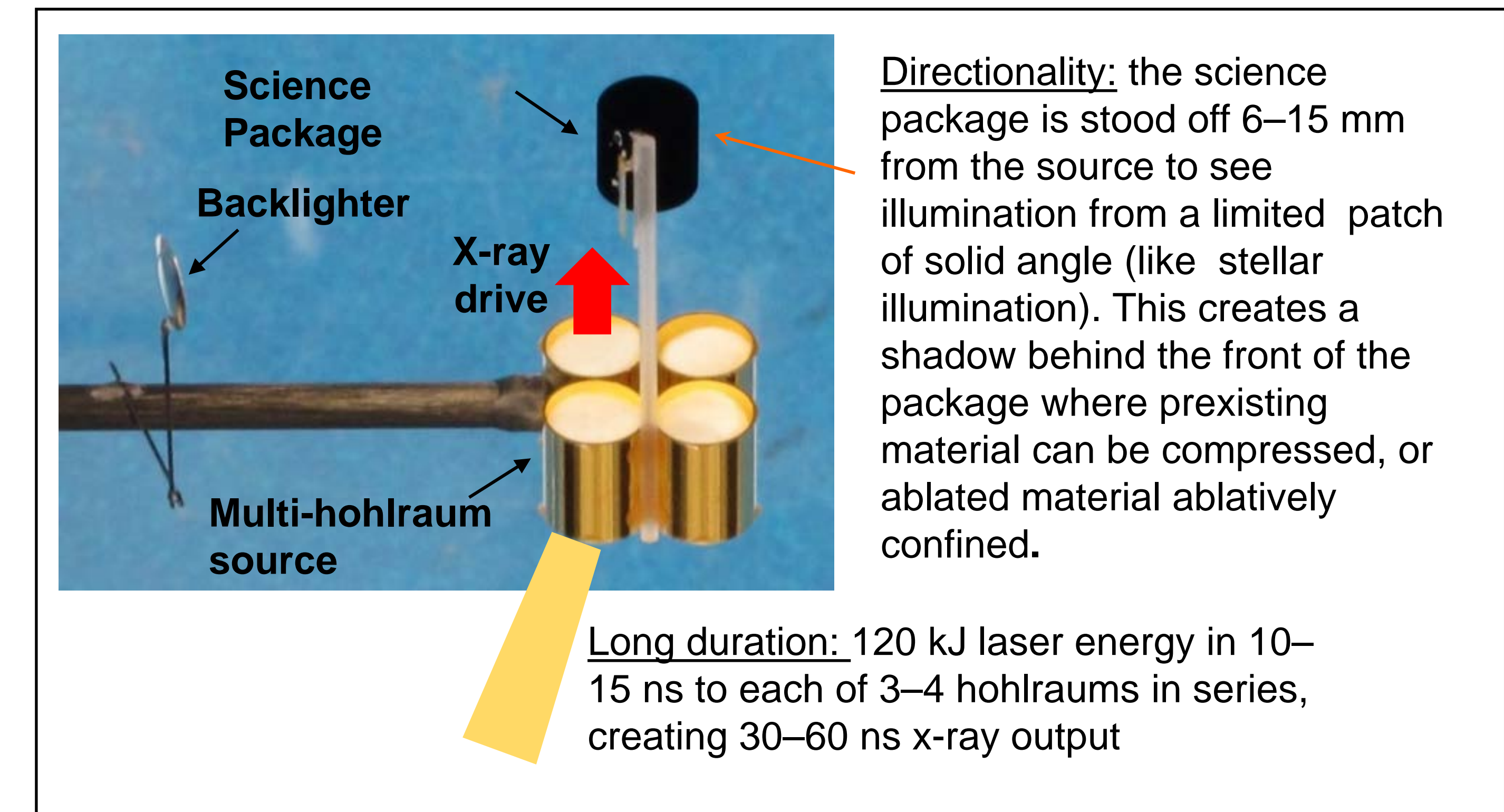
Observed gas velocity and column density as a function of projected distance in Eagle Pillar II (black symbols and lines) and in the two radiative hydrodynamic simulations (red lines). In the shielding model (right), both the column density and velocity reasonably match the observations, though the velocity in the simulated tail is too large. In the cometary model (left), the velocity is better matched. In both cases, the detailed results can be sensitive to initial parameters.



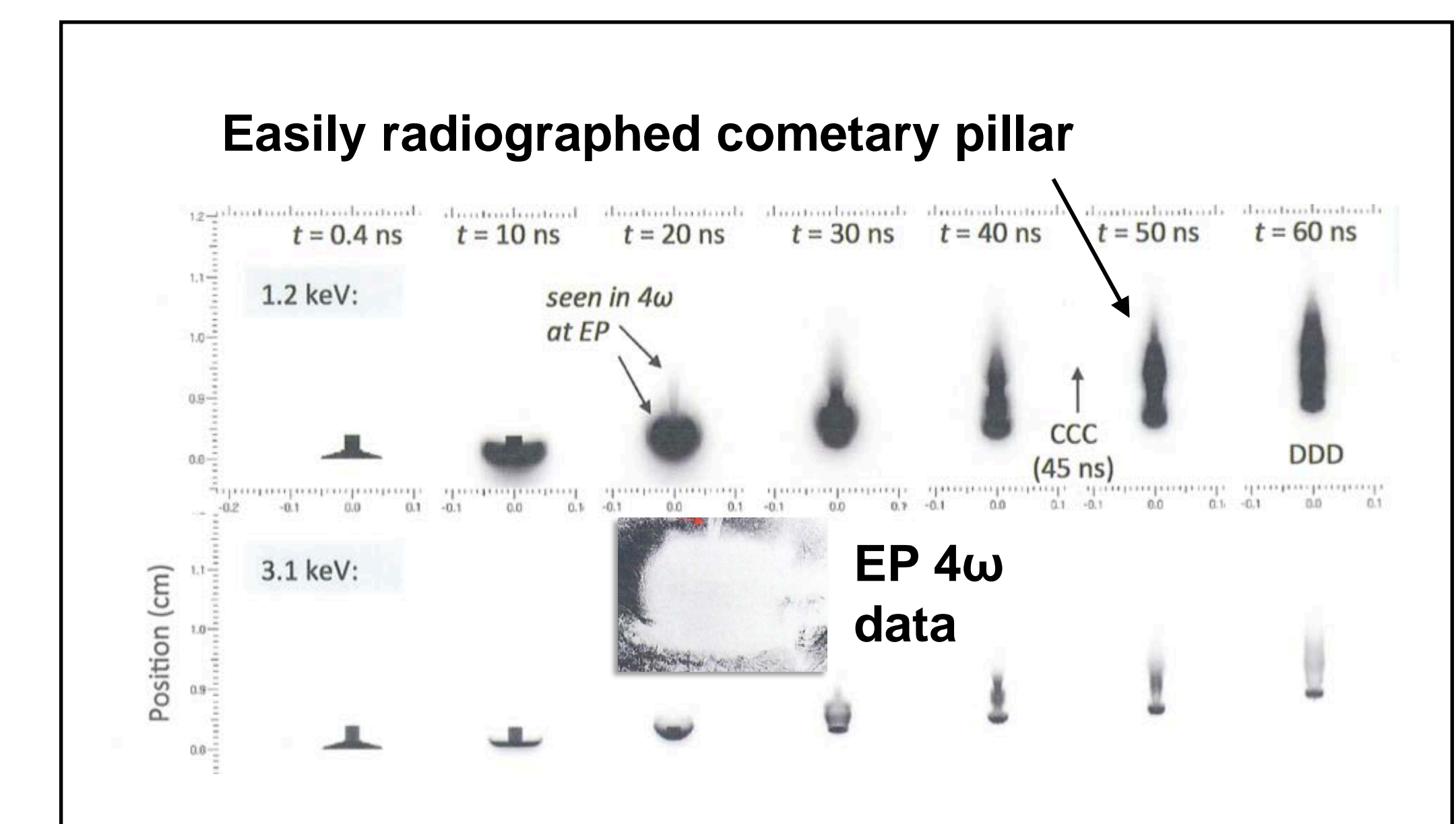
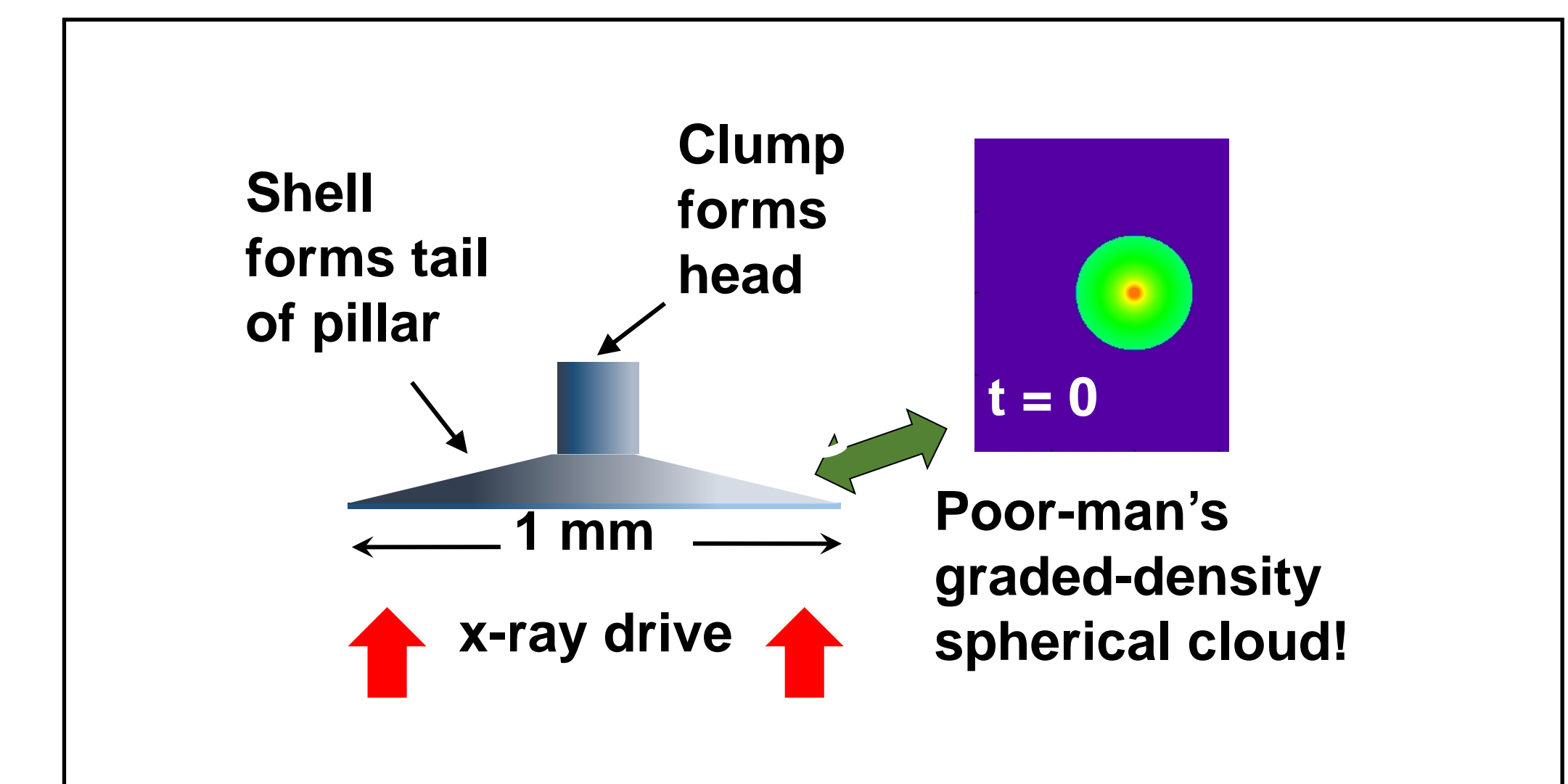
Snapshot from the cometary radiative hydrodynamic simulation after 250 kyr (right). In synthetic position-velocity diagram (left), the kinematic signature resembles the observational data, with a constant velocity head and accelerating tail. [12]. The relative flux in the simulated tail compared to the head appears lower than what we observe with CARMA.

## NIF DISCOVERY SCIENCE: EAGLE NEBULA

A novel multi-hohlraum, long duration (30-40 ns) directional source and science package were prototyped with three years of Laboratory Basic Science shots at the University of Rochester Laboratory for Laser Energetics Omega EP laser. In 2015, the first two NIF Discovery Science Eagle shots demonstrated the same source at 20x higher energy (240 kJ), generating backlit radiograph images of dense pillars formed from shielding targets. A cometary science package was prototyped at EP. For NIF DS, we will determine the column density and velocity structure of a true low-density cometary pillar formed at large standoff distance from a 480 kJ, 60+ ns x-ray source. Depending upon facility developments, we would to repeat the experiment with a coil-generated, static background magnetic field parallel to the axis of the evolving pillar and observe a broadening of the pillar diameter due to flux compression.



The new long duration, directional source: Multiple hohlraums are illuminated and then turned off in series, generating an x-ray output lasting up to 60 ns (so far). The source was prototyped with Laboratory Basic Science shots at Omega EP in FY13–15.



Proposed cometary science package for FY17–18 Eagle NIF shots. HYDRA predicts a simple machined CH target consisting of a conical shell in front of a clump will generate an easily radiographed long-lived cometary pillar. The shell is a ‘poor man’s’ version of the centrally condensed spherical cloud in the astrophysical simulations. Varying the backlighter energy allows viewing fainter vs. internal structure. Early evolution of prototype target was seen at Omega EP.

**REFERENCES:**

[1] Spitzer (1954)	[5] Williams+(2001)	[9] Lefloch & Lazareff (1994)
[2] Frieman (1954)	[6] Mizuta+ (2005,2006)	[10] Pound (1998)
[3] Axford (1964)	[7] Reipurth (1983)	[11] Reipurth & Bally (2003)
[4] Kane+ (2001)	[8] Bertoldi & McKee (1990)	[12] Pound+ (2007)

**ACKNOWLEDGEMENTS:**  
This work is supported by grants from the Department of Energy's High Energy Density Laboratory Physics program. CARMA operations and observations are supported by the National Science Foundation and the CARMA partners.